*J. Fluid Mech.* (2003), *vol.* 491, *pp.* 301–324.  
DOI: 10.1017/S0022112003005470 Printed in the United Kingdom

# Wave trapping and upstream influence in stratified flow of large depth

By DILIP PRASAD[1] AND T. R. AKYLAS[2]

[1]Aerodynamics Division, Pratt and Whitney Aircraft Engines, East Hartford, CT 06108, USA

[2]Department of Mechanical Engineering, Massachusetts Institute of Technology, Cambridge, MA 02139, USA

(Received 18 December 2002 and in revised form 7 April 2003)

A theoretical study is made of continuously stratified flow of large depth over topography when small periodic vertical fluctuations are present in the Brunt–Väisälä frequency, the background flow conditions being otherwise uniform. It is known from Phillips (1968) that, owing to nonlinear interactions with such fluctuations, internal gravity waves with vertical wavelength twice that of the background variations become trapped along the vertical, suggesting a waveguide-like behaviour. Using the asymptotic theory of Kantzios & Akylas (1993), we explore the role that this interaction-trapping mechanism plays in the generation of finite-amplitude long-wave disturbances near the hydrostatic limit. As a result of vertical trapping, a resonance phenomenon occurs and the linear hydrostatic response grows unbounded when the flow speed coincides with the long-wave speed of a free propagation mode that is trapped close to the ground. Near this critical flow speed, according to weakly nonlinear analysis, the wave evolution along the streamwise direction is governed by a forced extended Korteweg–de Vries equation, which predicts upstream-propagating solitary waves and bores similar to those obtained in resonant stratified flow of finite depth. The finite-amplitude response is then studied numerically and in some cases features strong upstream influence in the form of vertically trapped solitary waves and bores. On the other hand, incipient wave breaking is often encountered during the evolution of the nonlinear resonant response, and this flow feature, which is beyond the reach of weakly nonlinear theory, arises at topography amplitudes significantly below the critical value for overturning predicted by the classical model of Long (1953) for uniformly stratified steady flow.

## 1. Introduction

It was pointed out by Phillips (1968) that internal gravity waves in stratified fluids of large depth can be trapped in the vertical direction when small periodic vertical fluctuations are present in the background flow velocity and/or Brunt–Väisälä frequency. He considered in particular two oblique gravity wavetrains with the same horizontal but opposite vertical wavenumber components, and studied their interaction in nearly uniform background flow having small sinusoidal vertical variations of wavenumber twice the internal-wave vertical wavenumber. As a result of this special type of resonant-triad interaction, the amplitudes of the two gravity wavetrains drop off exponentially in the vertical direction over a lengthscale that is long compared with their vertical wavelength, but the mean-flow variations remain unaffected. Internal wave disturbances under these conditions may thus be trapped

close to the ground or ocean surface, their energy being essentially confined in a finite vertical region, suggesting a waveguide-like behaviour.

In the present study, we explore possible implications of this interaction-trapping mechanism for finite-amplitude internal wave disturbances generated by stratified flow of large depth over topography near the hydrostatic limit. This flow configuration is relevant in a variety of atmospheric and meteorological applications and has been the subject of numerous prior investigations (see, for example, Baines (1995) for a comprehensive survey). It is now well understood that the nature of the wave response can change significantly depending on whether the background flow conditions act as a waveguide of gravity waves. In a stratified fluid layer of finite depth, for instance, where energy is confined in the vertical direction, there is strong upstream influence, in the form of upstream-propagating solitary waves, when the flow speed is close to one of the long-wave speeds associated with the linear modes of propagation in the layer (Grimshaw & Smyth 1986). On the other hand, no such resonance phenomena occur in uniformly stratified (constant Brunt–Väisälä frequency) flow of large depth over topography, since energy can be freely radiated upwards under these flow conditions (Prasad, Ramirez & Akylas 1996).

In light of the trapping mechanism brought out by Phillips (1968), however, it is conceivable that small periodic variations in the background flow could alter the overall characteristics of uniformly stratified flow of large depth over topography. This issue is addressed here in the context of the asymptotic theory developed in Kantzios & Akylas (1993, hereinafter referred to as KA) for infinitely deep, nonlinear stratified flow near the hydrostatic limit (extended topography). In this flow geometry and under uniform background conditions (constant flow speed and Brunt–Väisälä frequency), the wave response takes the form of a slowly modulated columnar disturbance with fixed vertical wavenumber. To describe the dynamics of the flow, KA derived a pair of amplitude-evolution equations for this columnar disturbance, allowing for slight variations in the background velocity and density profiles. A special steady-state solution of these evolution equations for uniform background conditions corresponds to the celebrated Long's steady-flow state that was first obtained directly from the full Euler equations in steady form under the assumption of no upstream influence (Dubreil-Jacotin 1935; Long 1953). According to the theory of KA, Long's solution turns out to be linearly unstable at topography amplitudes well below the critical steady-state amplitude for overturning, but there is no evidence of upstream influence in the nonlinear transient flow (Prasad *et al.* 1996). This is in sharp contrast to the analogous finite-depth problem where, as already remarked, strong upstream influence in the form of solitary waves is observed under resonant-flow conditions (Grimshaw & Smyth 1986; Grimshaw & Yi 1991).

Motivated by the findings of Phillips (1968), here we revisit the generation of gravity waves by stratified flow of large depth over finite-amplitude topography, assuming that the background stratification is nearly uniform such that the Brunt–Väisälä frequency features small periodic vertical variations. This seemingly minor departure from uniform background flow conditions has a rather dramatic effect: owing to trapping of gravity waves in the vertical direction, infinitely deep stratified flow behaves, in many respects, like near-resonant flow in a waveguide. Specifically, in the absence of topography, there is a free mode that propagates along the streamwise direction but remains trapped close to the ground. When the flow speed coincides with the long-wave speed of this trapped mode, the linear forced response becomes unbounded, necessitating the consideration of nonlinear effects. Based on weakly nonlinear analysis, near this resonance, the wave evolution along the streamwise

direction is governed by a forced extended Korteweg–de Vries (eKdV) equation which combines cubic nonlinearity with third-order dispersion. At near-critical flow speeds, the weakly nonlinear response features upstream-propagating solitary waves and bores, similar to those found in resonant flow of finite depth (Grimshaw & Smyth 1986; Grimshaw, Chan & Chow 2002). These predictions are qualitatively consistent with numerical solutions of the fully nonlinear equations of KA under certain flow conditions. During the evolution of the nonlinear resonant response, however, we encounter wave breaking quite often, even when the topography amplitude is well below the critical value for overturning predicted by Long's model, and this flow feature cannot be captured by weakly nonlinear theory.

There is evidence from field observations that the Brunt–Väisälä frequency in the upper troposphere and lower stratosphere often features nearly periodic fluctuations so wave trapping could play a part in the propagation and breakdown of atmospheric gravity waves in those regions.

## 2. Review of asymptotic theory

We begin with a brief description of the finite-amplitude long-wave asymptotic theory of KA upon which the present study is based.

Consider two-dimensional flow of incompressible stratified fluid of unbounded vertical extent past a smooth obstacle of peak height $h_*$ and characteristic length $L_*$. The fluid velocity and Brunt–Väisälä frequency far upstream of the topography have characteristic values $U_*$ and $N_*$, respectively. Denoting by $g$ the acceleration due to gravity, the flow is characterized by the Boussinesq parameter $\beta = N_* U_*/g$, which is a measure of stratification, the nonlinearity parameter $\epsilon = N_* h_*/U_*$, which controls finite-amplitude effects, and the long-wave parameter $\mu = U_*/(N_* L_*)$, a measure of dispersive effects. In terms of these three parameters, the theory of KA applies to nearly hydrostatic ($\mu \ll 1$), nonlinear ($\epsilon = O(1)$), Boussinesq flow ($\beta \to 0$) under nearly uniform upstream flow conditions.

For uniform background flow velocity $U_*$ and Brunt–Väisälä frequency $N_*$, according to Long's model (Long 1953), the hydrostatic ($\mu \to 0$) finite-amplitude steady-flow response is a columnar disturbance that consists of a single mode with vertical wavenumber $N_*/U_*$ and has slowly varying amplitude in the streamwise direction. Motivated by this observation, KA pose the transient-flow response as a temporally and spatially modulated columnar disturbance with the same vertical wavenumber as Long's steady state, and derive a pair of evolution equations for the disturbance envelope, taking into account weak transient and dispersive (non-hydrostatic) effects as well as the presence of small variations in the background flow. As expected, these amplitude-evolution equations admit Long's state as a particular steady-state solution, and the theory of KA may thus be viewed as a generalization of Long's model near the hydrostatic limit.

More specifically, using dimensionless variables with $L_*/U_*$ as the timescale and $L_*$ and $U_*/N_*$, respectively, as the lengthscales along the streamwise ($-x$) and vertical ($-y$) directions, the streamfunction $\psi(x, y; Y, T)$ is written in the form

$$\psi = y + (A\mathrm{e}^{\mathrm{i}y} + \text{c.c.}) + O(\mu^2), \tag{2.1}$$

where c.c. denotes the complex conjugate. Consistent with the remarks made above, to leading order, the flow is the superposition of a uniform stream and a modulated columnar disturbance, the complex envelope $A(x, y, T) = a + \mathrm{i}b$ of which depends on the streamwise coordinate $x$, the stretched vertical coordinate $Y = \nu^2 y$ and the slow

time $T = \nu^2 t$, with $\nu = \alpha\mu$, $\alpha = O(1)$. Far upstream ($x \to -\infty$), where no disturbance is present, the background flow velocity and Brunt–Väisälä frequency are nearly uniform with $O(\nu^2)$ variations in the vertical direction:

$$\psi = y + \nu^2 r(y) \qquad (x \to -\infty), \tag{2.2a}$$

$$N^2(y) = 1 + \nu^2 q(y) \qquad (x \to -\infty). \tag{2.2b}$$

According to (2.1), the flow is quasi-steady and the background-flow conditions (2.2) depart only slightly from those for which Long's steady-flow model applies. This suggests replacing the vertical coordinate $y$ by $\psi$, exploiting the fact that, via this change of variable, the governing equations can be cast in linear form when Long's model is valid; the problem at hand may thus be tackled by perturbation methods. Of course, it should be kept in mind that the mapping $y = y(\psi; A)$ defined by (2.1) is unique provided flow reversal (wave breaking) does not occur, and this leads to the restriction

$$a^2 + b^2 < \tfrac{1}{4} \tag{2.3}$$

on the wave amplitudes $a$ and $b$.

Taking this approach, KA arrived at the following pair of coupled integral–differential evolution equations for the disturbance amplitudes $a$ and $b$:

$$\int_{-\infty}^{x} \mathrm{d}x' K_{11} a'_T + \int_{-\infty}^{x} \mathrm{d}x' K_{12} b'_T - \tfrac{1}{2}\alpha^2 a_{xx} + b_Y + N_1 = 0, \tag{2.4a}$$

$$\int_{-\infty}^{x} \mathrm{d}x' K_{21} a'_T + \int_{-\infty}^{x} \mathrm{d}x' K_{22} b'_T - \tfrac{1}{2}\alpha^2 b_{xx} - a_Y - N_2 = 0. \tag{2.4b}$$

The kernels $K_{11}, \ldots, K_{22}$ that enter the time-evolution terms above depend on $a$ and $b$ and are defined by

$$K_{11}(x, x') = \frac{1}{8\pi} \int_0^{2\pi} \mathrm{d}\psi \; y_a (y'_a + (y' y'_a)_\psi - y y'_{a\psi}), \tag{2.5a}$$

$$K_{12}(x, x') = \frac{1}{8\pi} \int_0^{2\pi} \mathrm{d}\psi \; y_a (y'_b + (y' y'_b)_\psi - y y'_{b\psi}), \tag{2.5b}$$

$$K_{21}(x, x') = \frac{1}{8\pi} \int_0^{2\pi} \mathrm{d}\psi \; y_b (y'_a + (y' y'_a)_\psi - y y'_{a\psi}), \tag{2.5c}$$

$$K_{22}(x, x') = \frac{1}{8\pi} \int_0^{2\pi} \mathrm{d}\psi \; y_b (y'_b + (y' y'_b)_\psi - y y'_{b\psi}), \tag{2.5d}$$

with the notation that primed variables are functions of $x'$. The terms $N_1$ and $N_2$ in (2.4) represent the effects brought about by the presence of small variations in the upstream flow conditions (2.2) and are given by

$$N_1 = \frac{1}{4\pi} \int_0^{2\pi} \mathrm{d}y \cos y \big\{ [r'' + r]_y^\psi + (\psi - y)(r' - q)|_\psi \big\}, \tag{2.6a}$$

$$N_2 = \frac{1}{4\pi} \int_0^{2\pi} \mathrm{d}y \sin y \big\{ [r'' + r]_y^\psi + (\psi - y)(r' - q)|_\psi \big\}. \tag{2.6b}$$

Note that the only possible sources of nonlinear terms in the evolution equations (2.4) are the kernels (2.5) that control transient effects and the terms $N_1$ and $N_2$ above; the steady-flow response under entirely uniform background flow conditions is thus governed by a linear equation system, consistent with Long's model.

The specification of the problem is completed by the boundary condition

$$a\cos\epsilon f - b\sin\epsilon f = -\tfrac{1}{2}\epsilon f, \qquad (Y=0); \tag{2.7}$$

in view of (2.1), this ensures that the topography profile $y=\epsilon f(x)$ is a streamline.

In the present study, we consider flow past the topographic profile known as the algebraic mountain (or 'Witch of Agnesi'), given by

$$f(x) = \frac{1}{1+x^2}. \tag{2.8}$$

As in Prasad *et al.* (1996), we also find it convenient here to work with the system of governing equations (2.4) after differentiating once with respect to $x$:

$$K^c_{11}a_T + K^c_{12}b_T + \int_{-\infty}^{x} \mathrm{d}x' \left(K_{11x}a'_T + K_{12x}b'_T\right) - \tfrac{1}{2}\alpha^2 a_{xxx} + b_{xY} + N_{1x} = 0, \tag{2.9a}$$

$$K^c_{21}a_T + K^c_{22}b_T + \int_{-\infty}^{x} \mathrm{d}x' \left(K_{21x}a'_T + K_{22x}b'_T\right) - \tfrac{1}{2}\alpha^2 b_{xxx} - a_{xY} - N_{2x} = 0, \tag{2.9b}$$

where $K^c_{ij} = K_{ij}(x,x)$. The hydrostatic limit of these equations, used by Prasad *et al.* (1996), is obtained by setting $\alpha = 0$.

Finally, the upstream flow conditions (2.2) are specified; for simplicity, it is assumed that no shear is present ($r \equiv 0$), but the Brunt–Väisälä frequency features sinusoidal fluctuations with vertical wavenumber twice that of the induced columnar disturbance (2.1):

$$q(y) = q_1 \sin 2y + q_2 \cos 2y. \tag{2.10}$$

We remark that this is precisely the resonance condition found by Phillips (1968) for the gravity-wave disturbance (2.1) to become trapped in the vertical direction owing to nonlinear interactions with periodic variations in the background flow. In the context of the evolution equations (2.9), as pointed out in KA, background flow variations with this particular period can give rise to wave trapping because, in the small-amplitude limit, the interaction terms $N_1$ and $N_2$ are linear in the disturbance amplitudes $a$ and $b$; for fluctuations of any other periodicity, $N_1$ and $N_2$ are nonlinear in $a$ and $b$ so interaction trapping is not possible.

## 3. Linear resonant response

It is instructive to study first the effects of the buoyancy fluctuations (2.10) on the wave response at small topographic amplitudes, $\epsilon \ll 1$. In this limit, the disturbance amplitudes $a$ and $b$ are small and the terms $N_1$ and $N_2$ in (2.6), that account for the background-flow variations, have the expansions

$$N_1 = -\tfrac{1}{4}q_2 a + \tfrac{1}{4}q_1 b + 2q_2 a^3 - 3q_1 a^2 b - q_1 b^3 + \ldots, \tag{3.1a}$$

$$N_2 = -\tfrac{1}{4}q_1 a - \tfrac{1}{4}q_2 b + q_1 a^3 + 3q_1 a b^2 + 2q_2 b^3 + \ldots. \tag{3.1b}$$

Likewise, the kernels $K_{11}, \ldots, K_{22}$ in (2.5), that control the time evolution of the disturbance amplitudes, can be expanded as follows:

$$K_{11} = 1 - 3(a^2 + a'^2) - (b^2 + b'^2) + 8(aa' + bb') + \ldots, \tag{3.2a}$$

$$K_{12} = -2(ab + a'b') - 8(a'b - ab') + \ldots, \tag{3.2b}$$

$$K_{21} = -2(ab + a'b') + 8(a'b - ab') + \ldots, \tag{3.2c}$$

$$K_{22} = 1 - (a^2 + a'^2) - 3(b^2 + b'^2) + 8(aa' + bb') + \ldots. \tag{3.2d}$$

In view of (3.1) and (3.2), the linearized versions of the evolution equations (2.9) are

$$a_T + b_{xY} - \tfrac{1}{2}\alpha^2 a_{xxx} - \tfrac{1}{4}q_2 a_x + \tfrac{1}{4}q_1 b_x = 0, \tag{3.3a}$$

$$b_T - a_{xY} - \tfrac{1}{2}\alpha^2 b_{xxx} + \tfrac{1}{4}q_1 a_x + \tfrac{1}{4}q_2 b_x = 0, \tag{3.3b}$$

and the boundary condition (2.7) reduces to

$$a = -\tfrac{1}{2}\epsilon f(x) \qquad (Y = 0). \tag{3.4}$$

In the absence of forcing ($\epsilon = 0$), it follows from (3.3) and (3.4) that for $q_1 > 0$, there is a free mode which propagates along the streamwise direction but remains trapped close to the ground ($Y = 0$):

$$a = 0, \qquad b = \exp\left(-\tfrac{1}{4}q_1 Y\right)\exp\{\mathrm{i}(kx - \omega T)\}, \tag{3.5}$$

and satisfies the linear dispersion relation

$$\omega = \tfrac{1}{4}q_2 k + \tfrac{1}{2}\alpha^2 k^3. \tag{3.6}$$

It is important to note that, according to (3.6), the long-wave speed associated with this trapped mode is $c_0 = q_2/4$ and is equal to the corresponding group velocity. From prior experiences (Akylas 1987), it is expected that this long-wave speed will then define a resonant-flow condition in the forced problem, analogous to that identified by Grimshaw & Yi (1991) in uniformly stratified flow in a channel of finite depth when the flow speed coincides with the phase speed of a hydrostatic mode of propagation. As verified below, this condition also obtains here, and the resonant flow speed which matches the long-wave speed of the trapped mode (3.5) is given, in dimensional variables, by

$$U_{\mathrm{crit}} = U_*\left(1 - \tfrac{1}{4}\mu^2 q_2\right), \tag{3.7}$$

where, in view of (2.10), $U_*$ is related to the vertical wavelength of the background-flow variations $\lambda_*$ via

$$U_* = \frac{\lambda_* N_*}{\pi}, \tag{3.8}$$

$N_*$ being the mean Brunt–Väisälä frequency. Moreover, according to (3.5), disturbances are trapped in the vertical direction over a distance $O(\lambda_*/\mu^2 q_1)$.

We now proceed to verify that, at resonant conditions, the linear hydrostatic response does not reach steady state, as was found by Grimshaw & Yi (1991) in the analogous finite-depth problem. In the non-dimensional formulation adopted here, for the purpose of studying the response near the critical flow speed (3.7), it is convenient to consider a reference frame moving with speed $c$, say,

$$\xi = x - cT, \tag{3.9}$$

and take the topography profile to be stationary in that frame, $y = \epsilon f(\xi)$; the condition for resonant flow then is $c = c_0 = q_2/4$. Implementing (3.9), the amplitude equations (3.3) in the hydrostatic limit ($\alpha \to 0$) become

$$a_T - (c + c_0)a_\xi + b_{\xi Y} + \tfrac{1}{4}q_1 b_\xi = 0, \tag{3.10a}$$

$$b_T + (c + c_0)b_\xi - a_{\xi Y} + \tfrac{1}{4}q_1 b_\xi = 0, \tag{3.10b}$$

while the boundary condition (3.4) reads

$$a = -\tfrac{1}{2}\epsilon f(\xi). \tag{3.11}$$

The steady-state solution of (3.10) that satisfies (3.11) and remains bounded as $Y \to \infty$, is

$$a = -\tfrac{1}{2}\epsilon f(\xi)\mathrm{e}^{-sY}, \tag{3.12a}$$

$$b = \tfrac{1}{2}\epsilon f(\xi)\frac{c + c_0}{s - \frac{1}{4}q_1}\mathrm{e}^{-sY}, \tag{3.12b}$$

where

$$s = \left(\tfrac{1}{16}\left(q_1^2 + q_2^2\right) - c^2\right)^{1/2}.$$

It is important to note that the steady-state solution for $b$ is singular if $s = q_1/4$ (for $c \neq -c_0$), which is the case when $c = c_0 = q_2/4$ and $q_1 > 0$; this is precisely the condition for resonant flow noted earlier, that occurs when the flow speed matches the long-wave speed of the trapped mode (3.5).

At resonant conditions ($c = c_0 = q_2/4$, $q_1 > 0$), it turns out that (3.12$b$) is replaced by

$$b = \tfrac{1}{4}\epsilon f(\xi)\left(q_1 T f_\xi - q_2 Y f\right)\exp\left(-\tfrac{1}{4}q_1 Y\right), \tag{3.13}$$

which reveals that $b$, in fact, grows linearly with $T$. It is worth noting that, in the analogous finite-depth problem, the linear hydrostatic response at resonance was also found to grow linearly with time (Grimshaw & Smyth 1986; Grimshaw & Yi 1991). This provides further evidence that, as a result of the interaction-trapping mechanism of Phillips (1968), vertically unbounded stratified flow can act as a waveguide when small periodic variations are present in the buoyancy frequency. Of course, as the linear resonant response grows unbounded, nonlinear effects will eventually become important close to resonance. We take up this issue in what follows.

## 4. Weakly nonlinear model

The theory of KA, outlined in § 2, is valid for $\epsilon = O(1)$ and can therefore be used to study the nonlinear flow response near resonance. Owing to the complexity of the governing equations (2.9), we must resort to a fully numerical approach for this purpose (see § 5). Before turning to a discussion of the nonlinear response, however, we shall derive a simplified evolution equation for small-amplitude disturbances. This weakly nonlinear model, although of limited validity, brings out more clearly the waveguide-like behaviour of vertically unbounded flow in the presence of periodic vertical variations.

Starting from the nonlinear amplitude equations (2.9) and the boundary condition (2.7) of the KA theory, we shall use a weakly nonlinear long-wave expansion ($\epsilon \ll 1$, $\alpha \ll 1$) to obtain a simplified evolution equation for nearly resonant flow ($c \approx c_0 = q_2/4$). The development here parallels that of Grimshaw & Smyth (1986) for resonant flow over topography in a channel of finite depth and only the salient features are described.

In preparation for the ensuing analysis, we adopt again the reference frame moving with speed $c$ according to (3.9) in which the topography is taken to be stationary. Making use of the integration properties of the kernels $K_{11}, \ldots, K_{22}$ described in Appendix A, the evolution equations (2.9) then transform to

$$K_{11}^c a_T + K_{12}^c b_T + \int_{-\infty}^{\xi} \mathrm{d}\xi'\left(K_{11\xi} a_T' + K_{12\xi} b_T'\right) - c a_\xi - \tfrac{1}{2}\alpha^2 a_{\xi\xi\xi} + b_{\xi Y} + N_{1\xi} = 0, \tag{4.1a}$$

$$K_{21}^c a_T + K_{22}^c b_T + \int_{-\infty}^{\xi} \mathrm{d}\xi'\left(K_{21\xi} a_T' + K_{22\xi} b_T'\right) - c b_\xi - \tfrac{1}{2}\alpha^2 b_{\xi\xi\xi} - a_{\xi Y} - N_{2\xi} = 0. \tag{4.1b}$$

Moreover, as before, the topography profile is taken to be $y = \epsilon f(\xi)$.

Taking $q_1 > 0$, close to resonance, we write

$$c = \tfrac{1}{4}q_2 - \alpha^2 c_1, \qquad c_1 = O(1); \tag{4.2}$$

recalling (3.7), the sign of the parameter $c_1$ determines whether the flow is supercritical ($c_1 > 0$) or subcritical ($c_1 < 0$). In the transcritical regime it turns out that the disturbance evolves on the slow time scale $\tau = \alpha^2 T$, and the appropriate expansions for $a$ and $b$ are

$$a = \alpha^{5/2} a_2 + \ldots, \qquad b = \alpha^{1/2}(b_0 + \alpha^2 b_2 + \ldots). \tag{4.3}$$

Furthermore, nonlinear and dispersive effects balance each other if $\epsilon = \alpha^{5/2}$, and the boundary condition (2.7) may therefore be written as

$$a = -\tfrac{1}{2}\alpha^{5/2} f(\xi) + \ldots \qquad (Y = 0). \tag{4.4}$$

We remark that, according to (4.3), the resonant response amplitude is $O(\alpha^{1/2})$ and hence much larger than the topography peak amplitude.

Inserting expansions (4.3) in the governing equations (4.1) and making use of the weakly nonlinear expressions (3.1) and (3.2) for $N_1$ and $N_2$ and the kernels $K_{11}, \ldots, K_{22}$, the solution at the lowest order is

$$b_0 = \mathscr{B}(\xi, \tau) \exp\left(-\tfrac{1}{4}q_1 Y\right), \tag{4.5}$$

$\mathscr{B}$ being an as yet undetermined amplitude. Proceeding to $O(\alpha^{5/2})$, it follows from (4.1$b$), making use of (3.1$b$) and (4.2), that $a_2$ satisfies the inhomogeneous equation

$$\left(a_{2Y} - \tfrac{1}{4}q_1 a_2\right)_\xi = \left(\mathscr{B}_\tau + c_1 \mathscr{B}_\xi - \tfrac{1}{2}\mathscr{B}_{\xi\xi\xi}\right) \exp\left(-\tfrac{1}{4}q_1 Y\right) - 2q_2 (\mathscr{B}^3)_\xi \exp\left(-\tfrac{3}{4}q_1 Y\right), \tag{4.6}$$

which, in view of (4.4), must be solved subject to the boundary condition

$$a_2 = -\tfrac{1}{2} f(\xi) \qquad (Y = 0). \tag{4.7}$$

For the above boundary-value problem to have a solution that remains bounded as $Y \to \infty$, the inhomogeneous terms in (4.6) and (4.7) must satisfy a compatibility condition that is readily obtained by multiplying (4.6) by its adjoint solution, $\exp(-q_1 Y/4)$, and integrating over $Y$ from 0 to $\infty$. Making use of the boundedness of $a_2$ as $Y \to \infty$ and the boundary condition (4.7), we then find that $\mathscr{B}$ must satisfy the amplitude equation

$$\mathscr{B}_\tau + c_1 \mathscr{B}_\xi - \tfrac{1}{2}\mathscr{B}_{\xi\xi\xi} - 3q_2 \mathscr{B}^2 \mathscr{B}_\xi = \tfrac{1}{4} q_1 f_\xi. \tag{4.8}$$

This is a particular version of the forced extended Korteweg–de Vries (eKdV) equation, in which third-order dispersive effects are balanced by a cubic nonlinearity. The more general form of this equation, which includes both quadratic and cubic nonlinearities, has been employed previously in studies of internal wave propagation in two-layer flows of finite depth (Kakutani & Yamasaki 1978; Miles 1979; Helfrich & Melville 1986). In the absence of forcing ($f = 0$), the eKdV equation has been shown by Kakutani & Yamasaki (1978) to admit solitary-wave and shock solutions. Grimshaw *et al.* (2002) have recently undertaken a comprehensive study of the general forced eKdV equation and interpreted the response in terms of a hydraulic approximation. It turns out that there is a rich variety of responses, featuring upstream influence in the form of solitary waves and bores.

The fully nonlinear computations in § 5 below indicate that the weakly nonlinear equation (4.8) is in fact quite restricted because, among other reasons, it cannot predict the onset of wave breaking. Accordingly, we shall present numerical solutions of (4.8)

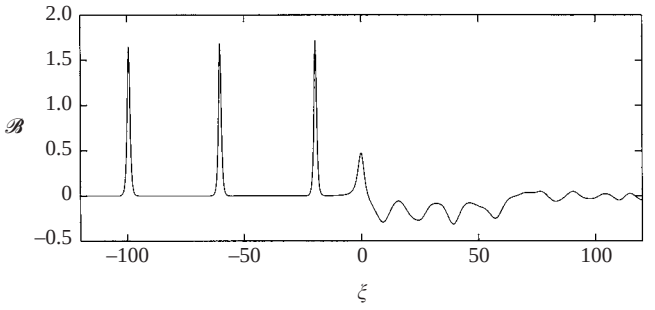


FIGURE 1. The wave amplitude $\mathscr{B}(\xi)$ at $\tau = 100$ for supercritical flow with $c_1 = 0.6$ and $q_1 = q_2 = \sqrt{2}$, illustrating the formation of upstream solitary waves.

only for a limited set of parameters, merely to illustrate that here also upstream influence is possible near resonant flow conditions.

The numerical method of solution of (4.8) is based on the Lax–Wendroff algorithm and is similar to that employed in § 5 for the full equations (see Appendix B). Specifically, the amplitude $\mathscr{B}$ is advanced from the $n$th to the $(n+1)$th time step according to

$$\mathscr{B}^{(n+1)} = \mathscr{B}^{(n)} + \mathscr{B}_\tau^{(n)} \Delta\tau + \tfrac{1}{2}\mathscr{B}_{\tau\tau}^{(n)} \Delta\tau^2,$$

where $\mathscr{B}_\tau^{(n)}$ is evaluated using (4.8), and the term involving $\mathscr{B}_{\tau\tau}^{(n)}$, which can be expressed in terms of spatial derivatives, provides the numerical damping necessary to maintain stability. In the present implementation, only linear terms in the expression for $\mathscr{B}_{\tau\tau}^{(n)}$ are retained so that the temporal accuracy is first- rather than second-order. The spatial derivatives are evaluated using centred second-order differences on a uniform grid, the spacing of which is set to $\Delta\xi = 0.05$. The method was validated by comparison with the results of Grimshaw *et al.* (2002) for the general forced eKdV equation.

We consider first supercritical flow with $c_1 = 0.6$ and $q_1 = q_2 = \sqrt{2}$. The solution at $\tau = 100$ is shown in figure 1. The upstream flow consists of a series of upstream-propagating solitary waves. Three such waves are visible in figure 1 and it is evident that a fourth solitary wave is in the process of forming above the obstacle, which is centred at $\xi = 0$. An undulating trough occurs immediately downstream followed by a dispersive wavetrain. The solitary waves are of relatively large amplitude and dominate the unsteady response.

Next, we consider flows with the stratification parameters $q_1 = \sqrt{2}$, $q_2 = -\sqrt{2}$. The wave amplitude $\mathscr{B}$ is shown in figure 2(*a*) at $\tau = 100$ for subcritical flow with $c_1 = -0.5$. We observe that a monotonic bore forms upstream of the obstacle. The downstream response consists of a uniform trough followed by a modulated lee wave of relatively large magnitude. The nature of the bore is sensitive to the value of $c_1$: when $c_1$ is decreased from $-0.5$ to $-0.75$, the monotonic bore becomes undular as shown in figure 2(*b*). The undular bore is weaker than its monotonic counterpart, while the strength of the lee wave field has increased. Both types of upstream-bore response are qualitatively similar to those of Grimshaw *et al.* (2002).

Finally, we examine a flow with $q_1 = q_2 = \sqrt{2}$ and $c_1 = -0.5$. The response at $\tau = 110$ is illustrated in figure 3. An oscillatory disturbance of decreasing amplitude propagates upstream. The downstream response consists of an irregular oscillatory wavetrain and can assume magnitudes considerably larger than that of the upstream wave.

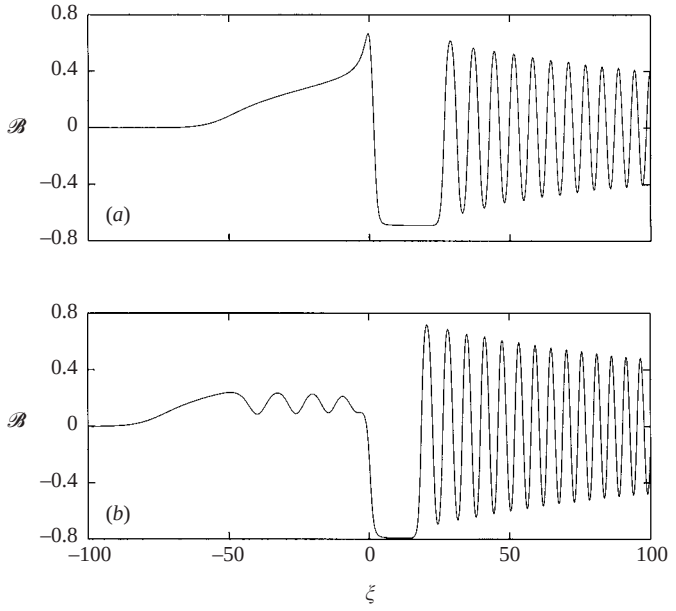


FIGURE 2. The wave amplitude $\mathscr{B}(\xi)$ at $\tau = 100$ for subcritical flow with $q_1 = \sqrt{2}$, $q_2 = -\sqrt{2}$: (*a*) $c_1 = -0.5$ and (*b*) $c_1 = -0.75$.

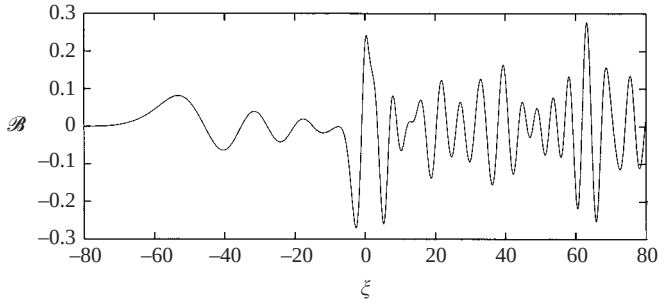


FIGURE 3. The wave amplitude $\mathscr{B}(\xi)$ at $\tau = 110$ for subcritical flow with $c_1 = -0.5$ and $q_1 = q_2 = \sqrt{2}$.

The preceding weakly nonlinear long-wave analysis illustrates the profound effect that periodic fluctuations in the background density distribution can have on the propagation of internal waves in a fluid of infinite depth under resonant flow conditions. In particular, these fluctuations cause trapping of the response close to the ground, resulting in flow behaviour entirely analogous to that of a confined system. The implications of this mechanism for the nonlinear flow response are explored below.

## 5. Nonlinear response

The evolution equation (4.8) describes the generation of very long ($\alpha \ll 1$) disturbances in the small-amplitude limit ($\epsilon \ll 1$). It is therefore clear that the onset of breaking, which occurs for finite-amplitude disturbances when condition (2.3) is

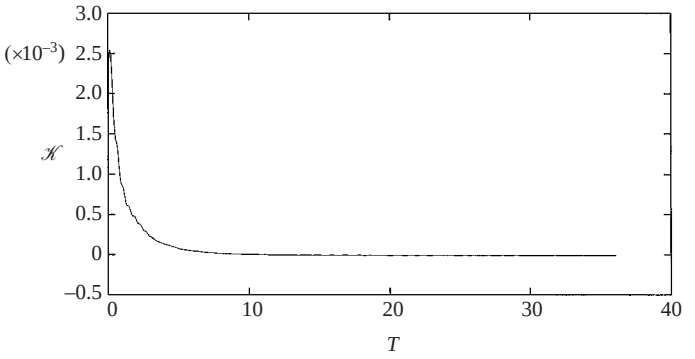


FIGURE 4. The rate of change of kinetic energy as a function of $T$ for flow past topography of amplitude $\epsilon = 0.1$ and stratification parameters $q_1 = -4\sqrt{2}$, $q_2 = 4\sqrt{2}$ at supercritical speed $c_1 = 1$.

first violated somewhere in the flow field, cannot be predicted using (4.8). In order to ascertain the possibility of overturning during the transient evolution of a fully nonlinear ($\epsilon = O(1)$) disturbance, it is necessary to solve the system of equations (4.1$a$, $b$) numerically. The procedure adopted for this purpose is based on the Lax–Wendroff algorithm and described in Appendix B.

Our interest here is centred on the transient response to the introduction of the obstacle. In order to avoid numerical difficulties associated with an impulsive start-up as well as to mimic the manner in which natural and laboratory flows are established, we assume that the obstacle is switched on gradually:

$$f(\xi, T) = \frac{1 - \mathrm{e}^{-40T}}{1 + \xi^2}. \tag{5.1}$$

According to (5.1), the obstacle attains 99.9% of its maximum amplitude before $T = 0.175$.

For uniformly stratified hydrostatic flow, Prasad *et al.* (1996) derived a global energy balance for the wave disturbance which proved useful in interpreting their numerical results. The modifications required to account for the effects of dispersion and varying background stratification are straightforward, and the energy balance again takes the form

$$\frac{\mathrm{d}}{\mathrm{d}t}\mathrm{KE} + \frac{\mathrm{d}}{\mathrm{d}t}\mathrm{PE} = \mathscr{R},$$

where the two terms on the left-hand side represent the rates of change of kinetic and potential energy, respectively, while $\mathscr{R}$ stands for the rate of work done by the force responsible for establishing the flow. In discussing the nonlinear flow response, we shall monitor the rate of change of kinetic energy, which can be expressed in terms of the disturbance amplitudes $a$ and $b$ as

$$\mathscr{K} \equiv \frac{\mathrm{d}}{\mathrm{d}t}\mathrm{KE} = \frac{\mathrm{d}}{\mathrm{d}T}\int_{-\infty}^{\infty} \mathrm{d}\xi \int_{0}^{\infty} \mathrm{d}Y (a^2 + b^2).$$

As indicated previously, the forced eKdV equation has recently been shown to possess a large variety of solutions (Grimshaw *et al.* 2002). It may then be expected that the present evolution equations (4.1$a$, $b$) are likely to yield a comparably

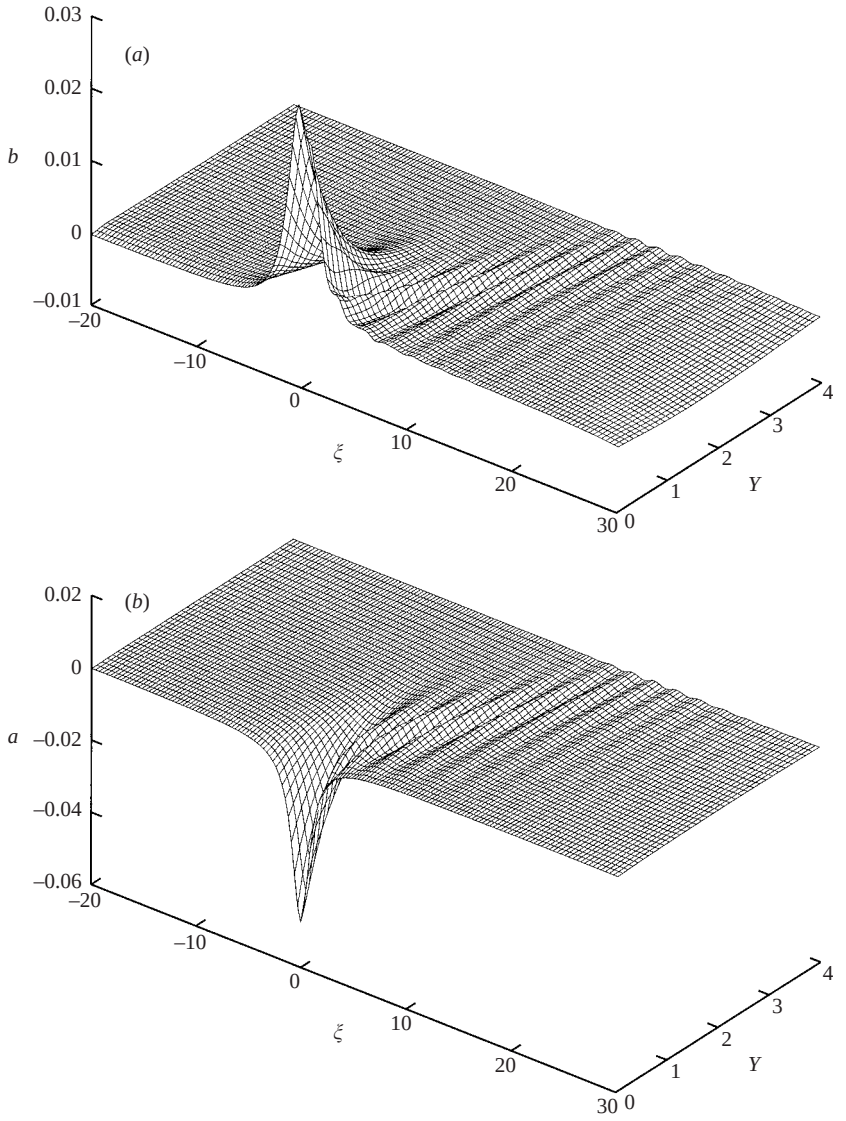


FIGURE 5. The wave amplitudes (*a*) $b(\xi, Y)$ and (*b*) $a(\xi, Y)$ at $T = 33.75$ for the flow parameters in figure 4.

rich solution set. However, owing to the computational expense associated with determining these solutions numerically, an exhaustive study will not be attempted. Instead, we present a few illustrative examples to demonstrate the behaviour of large-amplitude waves that cannot be described by the eKdV equation.

In solving the equation system (4.1*a*, *b*) subject to the boundary condition (2.7), we may, without loss of generality, set $\alpha = 1$ since $\alpha$ can be eliminated from 4.1($a$, $b$) via the rescalings $Y \to \alpha^2 Y$, $T \to \alpha^2 T$, $c \to c/\alpha^2$ and $(q_1, q_2) \to (q_1, q_2)/\alpha^2$. The flow conditions are thus specified by the nonlinear parameter $\epsilon$, the flow speed $c$ and the stratification parameters $q_1$ and $q_2$. As in the weakly nonlinear problem examined in § 4, we set the value of $c$ by prescribing $c_1$ in (4.2).

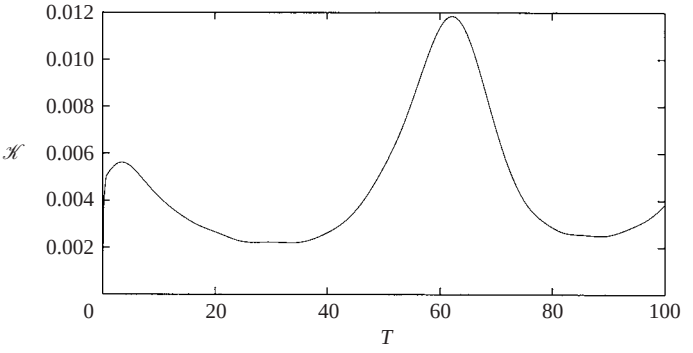


FIGURE 6. The rate of change of kinetic energy as a function of $T$ for flow past topography of amplitude $\epsilon = 0.1$ and stratification parameters $q_1 = q_2 = 4\sqrt{2}$ at supercritical speed $c_1 = 1$.

We consider first the supercritical-flow case $c_1 = 1$ with $q_1 = -4\sqrt{2}$, $q_2 = 4\sqrt{2}$ for the moderately small value of $\epsilon = 0.1$. Since $q_1$ is negative, it follows from (3.12$a$, $b$) that no resonance is possible and, on the basis of linear theory, a steady state should be achieved. We also recall that the forced eKdV equation is not relevant to this non-resonant flow regime. The evolution of the rate of change of kinetic energy $\mathscr{K}$ of the nonlinear response is shown as a function of $T$ in figure 4. Following the initial transient, we observe that $\mathscr{K}$ approaches zero at large $T$, indicating that a steady state is indeed attained. The wave amplitudes $b(\xi, Y)$ and $a(\xi, Y)$ are shown in figure 5 at $T = 33.75$. It is seen that $b$ and $a$ are of comparable magnitude and decay rapidly along the vertical direction, reflecting the trapped nature of the response. Furthermore, oblique dispersive waves are observed to form downstream of the obstacle, which is centred at $\xi = 0$. As expected, there is no evidence of upstream influence in the wave response.

We now consider a background stratification with $q_1 > 0$. In the discussion following (3.12), it was pointed out that under this condition, the linear hydrostatic flow becomes resonant. Here, we examine the dispersive nonlinear response for the choice of parameters $\epsilon = 0.1$ and $q_1 = q_2 = 4\sqrt{2}$ at a supercritical flow speed, $c_1 = 1$. The temporal evolution of $\mathscr{K}$, illustrated in figure 6, exhibits a strikingly different behaviour from that in figure 4. Following an initial period of relatively little variation, the rate of change of kinetic energy grows sharply at $T \approx 40$, achieving a rather large maximum value at $T \approx 62$. It then drops off rapidly, and another cycle appears to commence. The reason for the large variation in $\mathscr{K}$ can be understood by examining the wave amplitudes, which are shown in figure 7 at $T = 99.9$. Focusing on the amplitude $b(\xi, Y)$, we observe that solitary wave-like disturbances are generated upstream of the obstacle. At the instant shown, the first solitary wave has detached itself and propagated upstream, while the second is forming above the obstacle. Downstream of the obstacle, there are two depressions, followed by a dispersive lee-wavetrain with straight crests. The entire wave field is trapped close to the ground. The trapped nature of the wave response is also evident in the behaviour of the amplitude $a(\xi, Y)$. We note that although $a(\xi, Y)$ is confined close to $Y = 0$, the dependence on the vertical coordinate differs significantly from the non-resonant case, shown in figure 5. Further, the magnitude of $a$ is considerably smaller than that of $b$, consistent with the weakly nonlinear analysis presented in § 4. We remark, however, that the unsteady response shown in figure 7 is not truly weakly nonlinear. The nonlinearity of the wave disturbance can be measured in terms of the quantity $\eta = 4(a^2 + b^2)$;

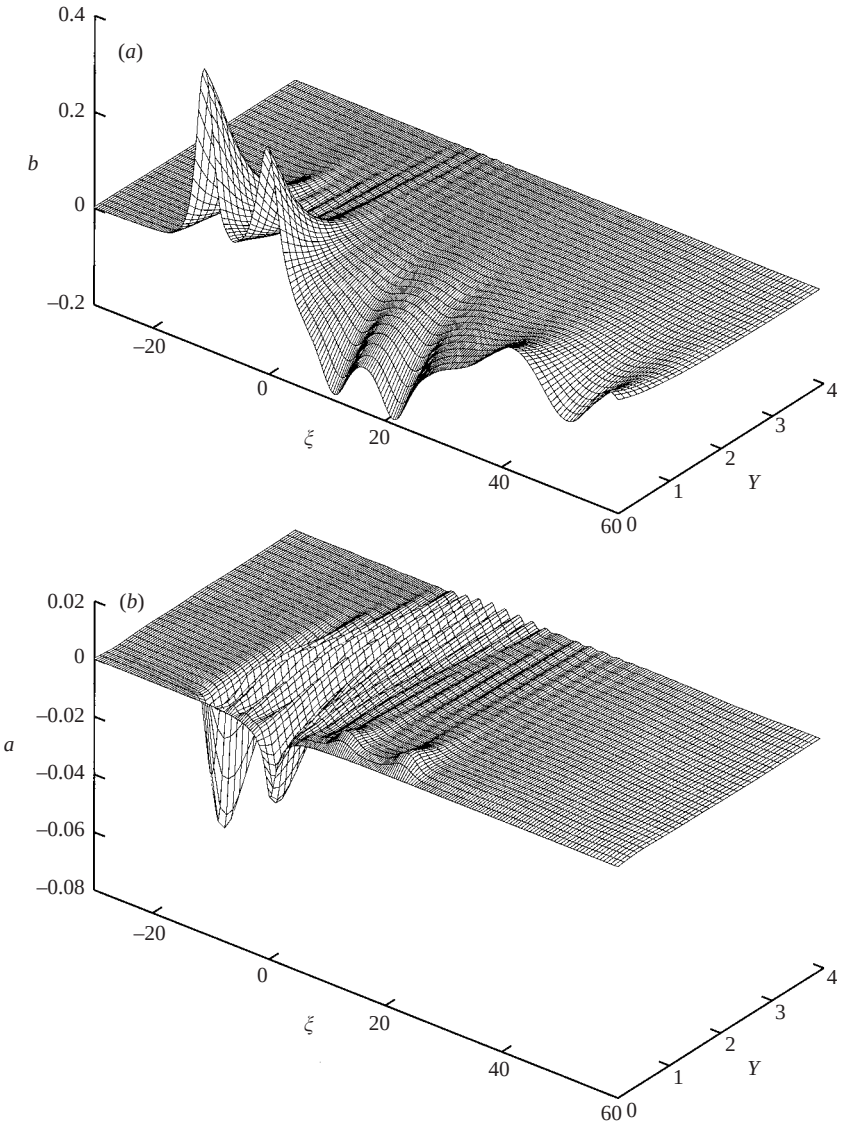


FIGURE 7. The wave amplitudes (*a*) $b(\xi, Y)$ and (*b*) $a(\xi, Y)$ at $T = 99.9$ for the flow parameters in figure 6.

according to (2.3), $\eta = 1$ at points in the flow field where the streamlines become vertical. The variation of $\eta$ with $\xi$ is shown in figure 8 on the lower boundary $Y = 0$ and along the lines $Y = 0.25, 0.5$. The amplitude of the wave, as measured by $\eta$ is seen to be quite large in the vicinity of the two solitary waves. The largest amplitude, corresponding to $\eta \approx 0.6$ is attained at the peak of the first solitary wave on $Y = 0$. In accordance with the trapped nature of the wave, $\eta$ drops off with $Y$, but its value on $Y = 0.5$ is still significant.

Under the same flow conditions as those in figure 8, the values of $\eta$ suggest that the critical overturning value of unity would probably be attained during the transient evolution of the response for a topography amplitude somewhat in excess of $\epsilon = 0.1$. As noted in Prasad *et al.* (1996), the kernels $K_{11}, \ldots, K_{22}$ become singular as $\eta \to 1$

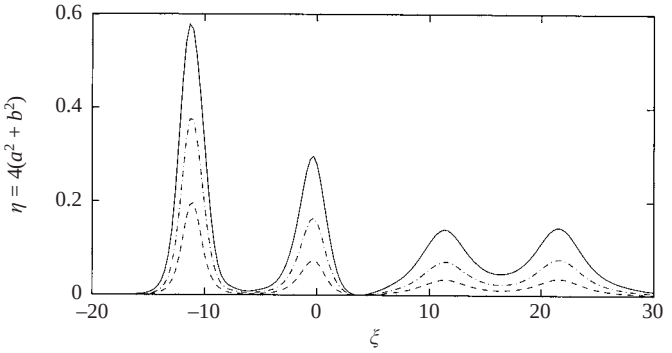


FIGURE 8. Variation of $\eta = 4(a^2 + b^2)$ with $\xi$ on $Y = 0$ (——), $Y = 0.25$ (– · – · –) and $Y = 0.5$ (– – –) for the flow parameters in figure 6.

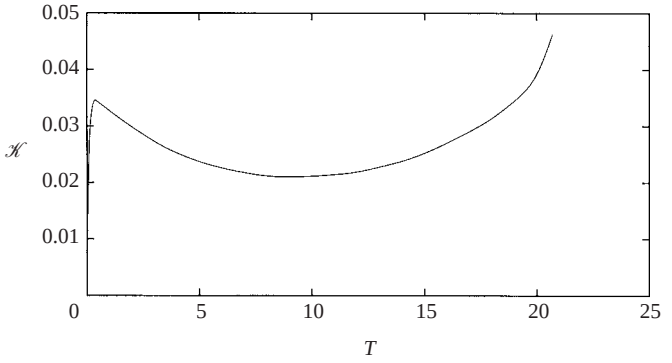


FIGURE 9. The rate of change of kinetic energy as a function of $T$ for flow past topography of amplitude $\epsilon = 0.3$ and stratification parameters $q_1 = q_2 = 4\sqrt{2}$ at supercritical speed $c_1 = 1.6$.

so nonlinear unsteady effects are expected to dominate the transient wave evolution when this critical value is approached. In the analogous finite-depth problem, a similar situation arises and, by integrating the governing finite-amplitude equation with improved resolution, Clarke & Grimshaw (1999) demonstrated that the effect of these unsteady nonlinear terms is to control the wave amplitude so as to keep $\eta < 1$, thus allowing the computation to proceed. On the other hand, the long-wave assumption ($\mu \ll 1$) employed in the derivation of their evolution equation as well as equations (4.1$a, b$) clearly breaks down when overturning is about to set in. In fact, numerical solutions of the full Euler equations for uniformly stratified nonlinear flow over topography (Rottman, Broutman & Grimshaw 1996) reveal that overturning does occur under flow conditions for which the finite-amplitude long-wave theory indicates that $\eta \to 1$, although the precise time of wave breaking is underestimated by the approximate theory. Accordingly, in the present computations, $\eta \to 1$ is interpreted as a sign that flow overturning will occur.

In order to investigate the possibility of overturning, we consider the flow past topography of amplitude $\epsilon = 0.3$ at a supercritical speed of $c_1 = 1.6$, with $q_1 = q_2 = 4\sqrt{2}$ as before. The behaviour of $\mathscr{K}$ with $T$ is shown in figure 9. The values of $\mathscr{K}$ are seen to be significantly higher than those in figure 6, indicating that the magnitudes of $a$ and $b$ are also larger. The evolution of $\mathscr{K}$ with $T$ bears similarities to that in figure 6; specifically, we observe that $\mathscr{K}$ begins to grow rapidly at $T \approx 12$, corresponding to

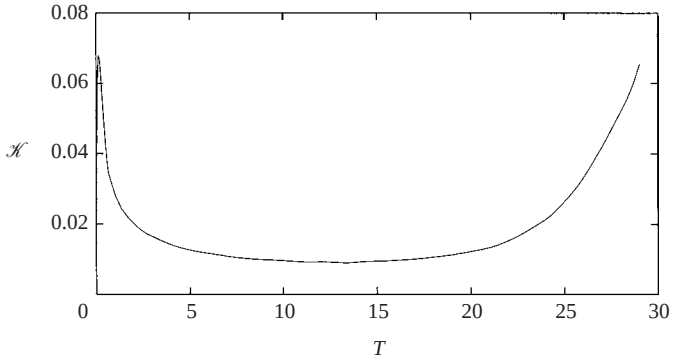


FIGURE 10. The rate of change of kinetic energy as a function of $T$ for flow past topography of amplitude $\epsilon = 0.5$ and stratification parameters $q_1 = -4\sqrt{2}$, $q_2 = 4\sqrt{2}$ at subcritical speed $c_1 = -2$.

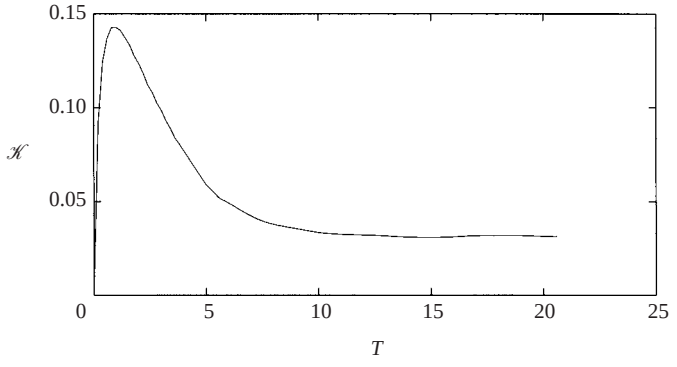


FIGURE 11. The rate of change of kinetic energy as a function of $T$ for flow past topography of amplitude $\epsilon = 0.5$ and stratification parameters $q_1 = 4\sqrt{2}$, $q_2 = -4\sqrt{2}$ at subcritical speed $c_1 = -0.8$.

the initial stages of solitary wave formation. However, incipient overturning is found at $T = 20.8$ before the solitary wave is released.

Next, we consider the flow past topography with $\epsilon = 0.5$ at a subcritical flow speed, $c_1 = -2$ and $q_1 = -4\sqrt{2}$, $q_2 = 4\sqrt{2}$. It has been shown that at small values of the topography amplitude ($\epsilon = 0.1$), the flow achieves a steady state, in accordance with linear theory. At the larger forcing amplitude, the rate of change of kinetic energy $\mathscr{K}$, shown in figure 10, exhibits a decay following the initial transient; however, unlike the small-amplitude case, the value of $\mathscr{K}$ remains finite during this period. At $T \approx 15$, $\mathscr{K}$ begins to increase, leading to rapid growth of the amplitudes $a$ and $b$, which results in wave breaking at $T = 29.3$. Thus, the presence of nonlinearity in this instance has a destabilizing effect on a flow that would be predicted to achieve a steady state on the basis of linear theory.

In the cases examined thus far, attention has been restricted to positive values of $q_2$. We now consider a subcritical flow with $c_1 = -0.8$ past topography of amplitude $\epsilon = 0.5$, with stratification parameters $q_1 = 4\sqrt{2}$ and $q_2 = -4\sqrt{2}$. The rate of change of kinetic energy is shown in figure 11. There is a slow growth of $\mathscr{K}$ initially that does not appear to be associated with the startup transient. At large $T$, the rate of change of kinetic energy approaches a finite value, indicating that the flow remains unsteady.

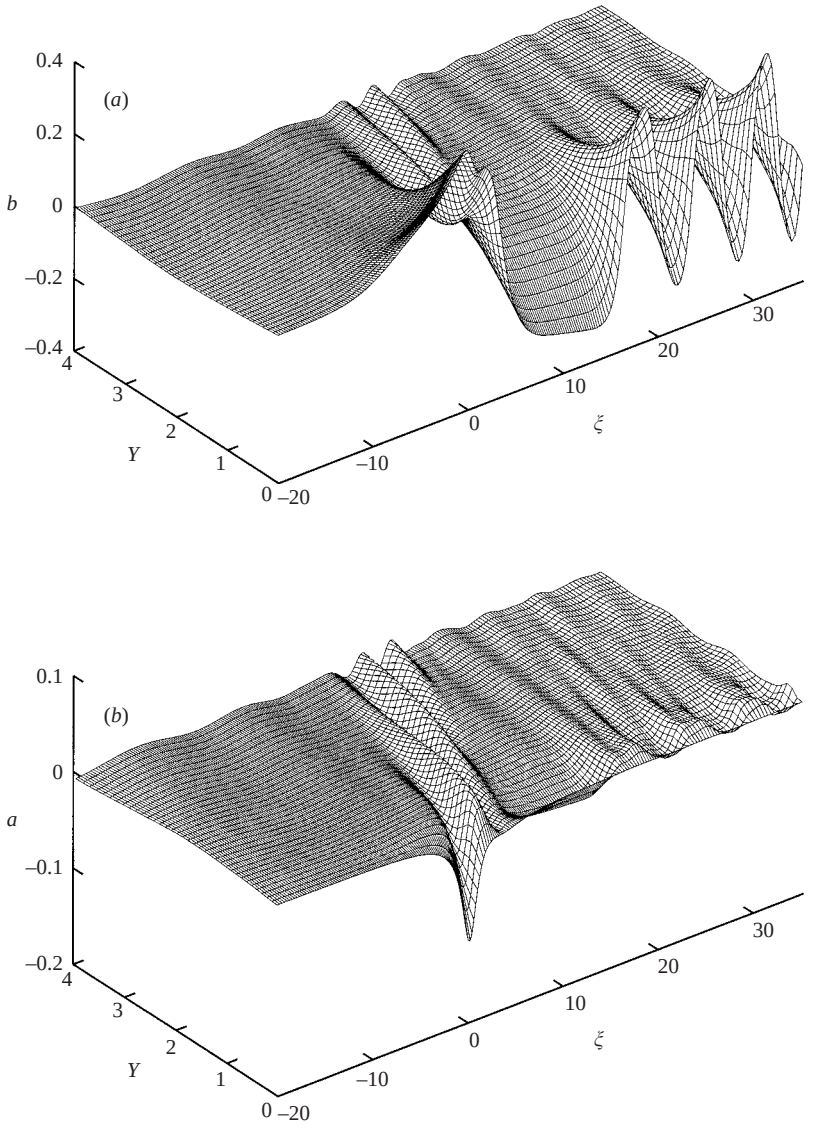


FIGURE 12. The wave amplitudes (*a*) $b(\xi, Y)$ and (*b*) $a(\xi, Y)$ at $T = 20$ for the flow parameters in figure 11.

The wave amplitudes, $b(\xi, Y)$ and $a(\xi, Y)$ are illustrated in figure 12 at $T = 20$. The amplitude $b$ features an upstream bore, followed by a trough that lengthens with time. The flow downstream is dominated by a vertically trapped lee wave. Although these phenomena are qualitatively similar to the weakly nonlinear results of § 4 for $q_1 = \sqrt{2}$, $q_2 = -\sqrt{2}$ and subcritical flow speeds, it is important to note that the response here is fully nonlinear. In fact, setting $c_1$ to a value comparable to that in the weakly nonlinear case shown in figure 2(*a*) results in wave breaking before the formation of a bore. Note that while the downstream disturbance is straight-crested, the bore itself has crests that are oblique to the ground, which is particularly evident in the variation of $a(\xi, Y)$.

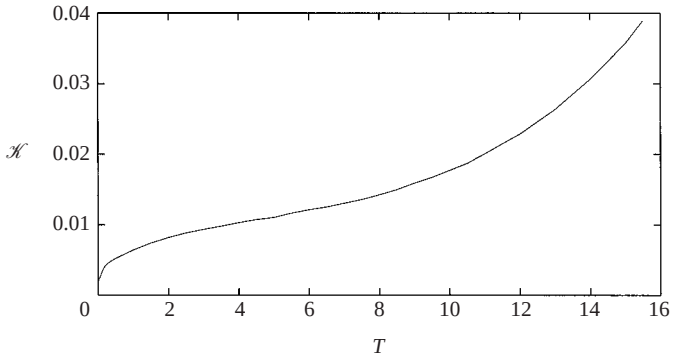


FIGURE 13. The rate of change of kinetic energy as a function of $T$ for flow past topography of amplitude $\epsilon = 0.1$ and stratification parameters $q_1 = q_2 = 4\sqrt{2}$ at subcritical speed $c_1 = -0.4$.

As a final example, we consider a subcritical flow with $c_1 = -0.4$ and $q_1 = q_2 = 4\sqrt{2}$ past topography of amplitude $\epsilon = 0.1$. This may be regarded as the analogue of the weakly nonlinear flow examined in figure 3 of §4. The rate of change of kinetic energy $\mathscr{K}$, shown in figure 13, exhibits a continuous increase until incipient breaking is encountered at $T = 15.7$. The wave amplitudes $a$ and $b$ are shown in figure 14 just prior to the occurrence of overturning at $T = 15$. A dispersive wavetrain is formed downstream of the obstacle. We also observe that a steep trough in $b$ is generated immediately downstream of the obstacle, which is also associated with a peak in $a$. As evidenced by the behaviour of $\mathscr{K}$ in figure 13, these extrema continue to grow until the breaking criterion is achieved. It is notable that this occurs even for the relatively small topography amplitude of $\epsilon = 0.1$, emphasizing that the presence of vertical mean flow variations can have a major impact on the unsteady flow.

## 6. Discussion

This study has revisited the classical problem of stratified flow of large depth over two-dimensional topography assuming that the Brunt–Väisälä frequency features small periodic vertical variations, the background conditions being otherwise uniform. Phillips (1968) pointed out that, as a result of their interaction with such non-uniformities, internal waves in an unbounded stratified fluid can be trapped in the vertical direction when their vertical wavelength is twice that of the underlying flow variations, suggesting a waveguide-like behaviour. In the flow configuration studied here, this interaction-trapping mechanism leads to a resonance phenomenon when the background flow speed coincides with the long-wave speed of a free mode that propagates along the horizontal direction but is trapped close to the ground. The linear resonant response grows without bound and, as in other forced wave problems where similar resonances arise (Akylas 1987), nonlinear effects come into play near this critical flow speed. These effects were first studied in the weakly nonlinear regime and it was found that the evolution of the trapped-mode amplitude is described by a forced eKdV equation with cubic nonlinearity. This is analogous to the waveguide behaviour observed in resonant stratified flows of finite depth (Grimshaw & Smyth 1968; Grimshaw & Yi 1991) and is a consequence of the trapping brought about by the background flow variations, which confines the wave energy over a finite vertical distance. Numerical solutions of the forced eKdV equation demonstrate the existence of upstream influence in the form of solitary waves and bores.

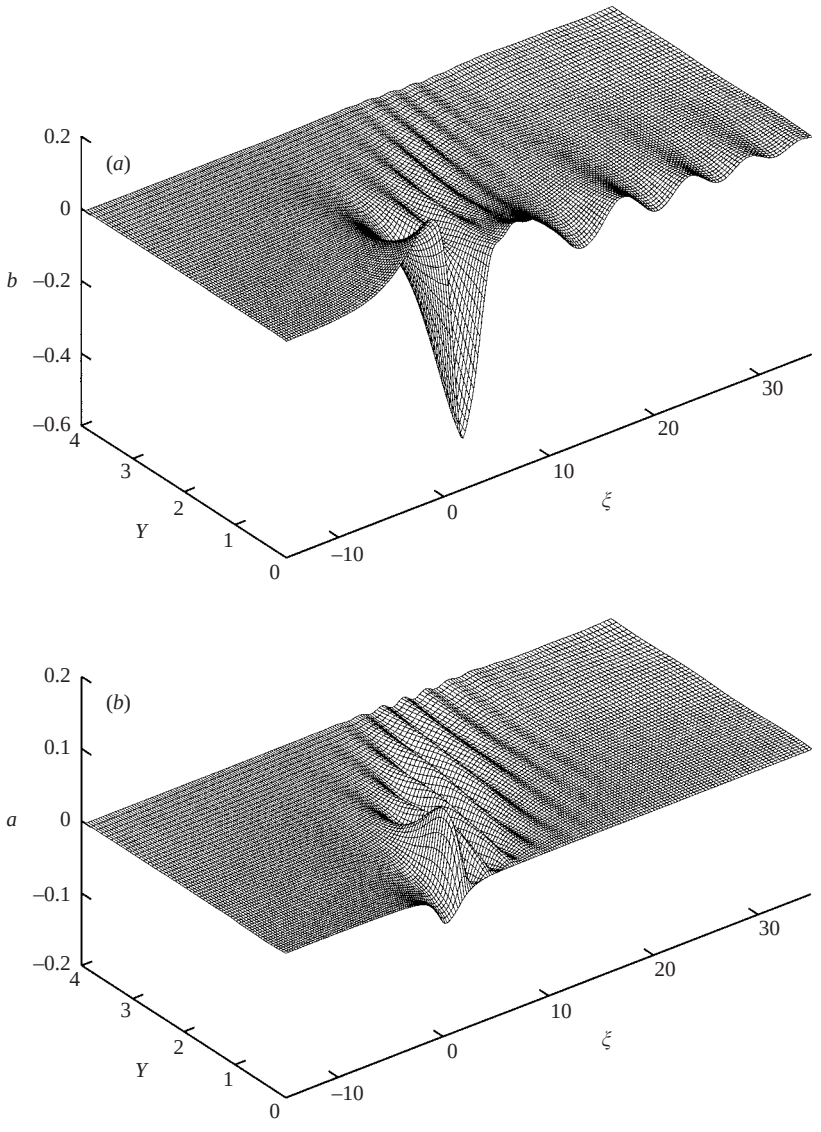


FIGURE 14. The wave amplitudes (*a*) $b(\xi, Y)$ and (*b*) $a(\xi, Y)$ at $T = 15$ for the flow parameters in figure 13.

Under the flow conditions assumed here, it is also feasible, based on the amplitude-evolution equations derived in KA, to examine the resonant flow response over topography of finite amplitude near the hydrostatic limit, as long as overturning has not occurred. These evolution equations were solved numerically for flow past the algebraic mountain. In the absence of background flow non-uniformities and assuming no upstream influence, the steady flow response is described by Long's (1953) model. For the algebraic mountain in the hydrostatic limit, Long's steady state first features vertical streamlines, signalling the onset of overturning, at the critical topography amplitude $\epsilon = 0.85$. Moreover, the corresponding transient flow does not exhibit upstream influence and there is no occurrence of breaking for topography amplitudes below this critical value (Prasad *et al.* 1996). The present

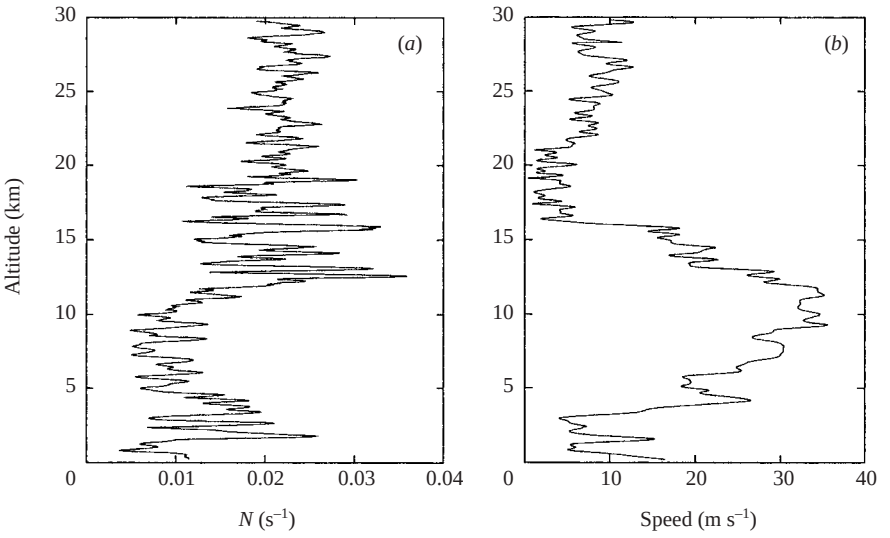


FIGURE 15. Balloon measurements taken in the lee of Mt. Washington illustrating the (*a*) Brunt–Väisälä frequency, and (*b*) flow speed as a function of altitude.

study has revealed, however, that a small periodic non-uniformity in the Brunt–Väisälä frequency can have a profound effect on the unsteady response. In particular, it was shown that the upstream-propagating solitary waves and bores observed in the weakly nonlinear case possess finite-amplitude counterparts and, further, that breaking occurs over a broad range of flow conditions. These phenomena are present even at topography amplitudes well below the critical value for overturning predicted by Long's model.

Although the form of the variable background stratification considered here is of a rather special type, similar effects can be expected to occur for more general flow non-uniformities as well. Specifically, it would suffice for the Brunt–Väisälä frequency to feature nearly periodic variations and only within the vertical region into which the trapped disturbances are confined. Moreover, as envisaged by Phillips (1968), it is clear from (2.6) that non-uniformities of a similar form in the background velocity profile would also lead to wave trapping.

The preceding analysis suggests that the effects of interaction trapping on stratified flow over topography are quite robust and should therefore be detectable in field or laboratory measurements. Although we know of no detailed measurements pertaining specifically to the present theory, we display in figure 15 atmospheric data obtained from balloon measurements performed by the Air Force Research Laboratory (Hanscom Air Force Base) in the lee of Mount Washington on 31 May 2001 under relatively steady flow conditions. Focusing attention on figure 15(*a*), we observe that the values of the Brunt–Väisälä frequency oscillate about a mean which ranges roughly between 0.01 and $0.03\,\mathrm{s}^{-1}$, and the fluctuations have typical wavelengths of the order of 1–2 km. Although the departures from the 'mean' are quite large here, the resonant wind speed (3.7) predicted by the present theory based on these data lies between 5 and $20\,\mathrm{m\,s}^{-1}$, which is within the range of the flow speed profile shown in figure 15(*b*). We note, however, that detailed measurements in a controlled setting are necessary to confirm the validity of the theoretical predictions in a definitive manner.

The authors are indebted to Dr Robert Beland and his group at the Air Force Research Laboratory at Hanscom AFB for several useful discussions on this and related topics and for providing the data depicted in figure 15. Financial support provided to TRA by the Air Force Office of Scientific Research, Air Force Materials Command, USAF, under Grant F49620-01-1-001 and by the National Science Foundation under Grant DMS-0072145 is gratefully acknowledged.

## Appendix A. Kernel integration properties

Here, we demonstrate the reduction property of the kernels $K_{11}, \ldots, K_{22}$ that was used to obtain the evolution equations (4.1) in the reference frame (3.9). This property is similar to that of the single kernel which appears in the analogous finite-depth problem (Grimshaw & Yi 1991). Considering the expressions (2.5$a$, $b$) for $K_{11}$ and $K_{12}$, we find upon integrating the second terms of the integrand by parts that

$$K_{11} = \frac{1}{8\pi}\int_0^{2\pi} \mathrm{d}\psi (y_a y'_a - y_{a\psi} y' y'_a - y_a y y'_{a\psi}),$$

$$K_{12} = \frac{1}{8\pi}\int_0^{2\pi} \mathrm{d}\psi (y_a y'_b - y_{a\psi} y' y'_b - y_a y y'_{b\psi}).$$

Making use of the relation $y = y(\psi; a, b)$, we may write

$$y_x|_\psi = y_a a_x + y_b b_x,$$

which yields the following simplification:

$$\int_{-\infty}^{x} \mathrm{d}x'[K_{11}a'_x + K_{12}b'_x] = \frac{1}{8\pi}\int_0^{2\pi} \mathrm{d}\psi \int_{-\infty}^{x} \mathrm{d}x' \left[y_a y'_x|_\psi - \tfrac{1}{2} y_{a\psi}(y'^2)_x|_\psi - y y_a (y'_\psi)_x|_\psi\right].$$

Evaluating the integrals on the right-hand side of the above expression, we find that

$$\int_{-\infty}^{x} \mathrm{d}x'[K_{11}a'_x + K_{12}b'_x] = \frac{1}{4\pi}\int_0^{2\pi} \mathrm{d}\psi\, y_a(y-\psi),$$

$$= \frac{1}{\pi}\int_0^{2\pi} \mathrm{d}\psi\, y_\psi \cos y(a\cos y - b\sin y).$$

The final integration is readily accomplished and we find that

$$\int_{-\infty}^{x} \mathrm{d}x'[K_{11}a'_x + K_{12}b'_x] = a.$$

In a similar manner, it may be shown that

$$\int_{-\infty}^{x} \mathrm{d}x'[K_{21}a'_x + K_{22}b'_x] = b.$$

## Appendix B. Numerical method

In this Appendix, a brief description of the numerical method used to solve the evolution equations (4.1$a$, $b$) is given. The integral–differential nature of these equations suggests the use of an explicit method. In the present study, the wave amplitudes, $a$ and $b$, are discretized using finite differences on a non-uniform grid $(\xi_i, Y_j)$. All spatial derivatives in the interior of the domain are evaluated using centred, second-order stencils and the integral terms are evaluated using the trapezoidal rule.

The solution is advanced in time using a scheme that is similar to the Lax–Wendroff method. The discretized forms of (4.1$a$, $b$) may be written as

$$\mathbf{K}\boldsymbol{u}_T = \mathbf{L}\boldsymbol{u}_{\xi Y} - \mathbf{Q}\boldsymbol{u}_\xi + \tfrac{1}{2}\alpha^2\boldsymbol{u}_{\xi\xi\xi} + \text{'nlt'}, \tag{B 1}$$

where $\boldsymbol{u}$ is a column vector with entries $a_{i,j}$ and $b_{i,j}$, 'nlt' stands for nonlinear terms and the matrix operators $\mathbf{K}$, $\mathbf{L}$ and $\mathbf{Q}$ are defined by

$$\mathbf{K} = \begin{bmatrix} K_{11}^c + \frac{1}{2}K_{11\xi}\Delta\xi & K_{12}^c + \frac{1}{2}K_{12\xi}\Delta\xi \\ K_{21}^c + \frac{1}{2}K_{21\xi}\Delta\xi & K_{22}^c + \frac{1}{2}K_{22\xi}\Delta\xi \end{bmatrix}_{(ij)},$$

$$\mathbf{L} = \begin{bmatrix} 0 & -1 \\ 1 & 0 \end{bmatrix}, \qquad \mathbf{Q} = \tfrac{1}{4}\begin{bmatrix} -4c - q_2 & q_1 \\ q_1 & -4c + q_2 \end{bmatrix}.$$

Here, $\Delta\xi$ is the grid spacing along the $\xi$-direction and is, in general, not uniform. It may then be shown from (B 1) that

$$\begin{aligned} \mathbf{K}\boldsymbol{u}_{TT} = {} & (\mathbf{L}\mathbf{K}^{-1}\mathbf{L})\boldsymbol{u}_{\xi\xi YY} + (\mathbf{Q}\mathbf{K}^{-1}\mathbf{Q})\boldsymbol{u}_{\xi\xi} + \tfrac{1}{4}\alpha^4\mathbf{K}^{-1}\boldsymbol{u}_{\xi\xi\xi\xi\xi\xi} \\ & - (\mathbf{L}\mathbf{K}^{-1}\mathbf{Q} + \mathbf{Q}\mathbf{K}^{-1}\mathbf{L})\boldsymbol{u}_{\xi\xi Y} + \tfrac{1}{2}\alpha^2(\mathbf{L}\mathbf{K}^{-1} + \mathbf{K}^{-1}\mathbf{L})\boldsymbol{u}_{\xi\xi\xi\xi Y} \\ & - \tfrac{1}{2}\alpha^2(\mathbf{Q}\mathbf{K}^{-1} + \mathbf{K}^{-1}\mathbf{Q})\boldsymbol{u}_{\xi\xi\xi\xi} + \text{'nlt'}. \end{aligned} \tag{B 2}$$

The wave amplitudes are advanced from the $n$th to the $(n+1)$th time step according to

$$\boldsymbol{u}^{(n+1)} = \boldsymbol{u}^{(n)} + \boldsymbol{u}_T^{(n)}\Delta T + \tfrac{1}{2}\boldsymbol{u}_{TT}^{(n)}\Delta T^2, \tag{B 3}$$

where $\Delta T$ is the time step. Equation (B 3), together with (B 1) and (B 2) represent the Lax–Wendroff algorithm, which is conditionally stable and second-order accurate in both space and time. However, direct implementation of this method would prove to be computationally expensive owing to the presence of the nonlinear terms in (B 2). Furthermore, these terms are not required to maintain numerical stability, which is ensured by the linear terms. We therefore neglect the nonlinear terms in (B 2). Moreover, numerical experiments show that retention of the first three terms on the right-hand side of (B 2) is sufficient to ensure stability and therefore the remaining linear terms are excluded as well.

These modifications minimize the numerical damping, but result in a scheme with first-order rather than second-order temporal accuracy. Upon carrying out a von Neumann analysis of the scheme (B 3) applied to the linearized governing equations, it is found to be stable provided

$$\Delta T \leqslant O(\Delta\xi\,\Delta Y),\ O(\Delta\xi^3),$$

where $\Delta Y$ is the grid spacing along the $Y$-direction. In practice, we generally choose $\Delta Y \sim \Delta\xi$, so the stability requirement is $\Delta T \leqslant O(\Delta\xi^3)$. Hence, a fine-grid resolution ensures that the time step $\Delta T$ is small and the first-order temporal accuracy of the scheme is not a significant issue. The typical values of $\Delta\xi$ and $\Delta Y$ employed in the present simulations were in the ranges 0.2–0.3 and 0.05–0.1, respectively. Furthermore, care was taken to ensure that changes in the grid spacing were sufficiently smooth so as to avoid spurious numerical reflections.

The values of the kernels required to evaluate the right-hand side of (B 3) are determined explicitly. In order to reduce the computational cost associated with determining the kernels, the procedure of Prasad *et al.* (1996) is adopted. Specifically, the linear limits $K_{11} = K_{22} = 1$, $K_{12} = K_{21} = 0$ are used for values of $a^2 + b^2 + a'^2 + b'^2$

less than a lower threshold value of 0.005. When $a^2+b^2+a'^2+b'^2$ exceeds an upper threshold of 0.05, the integrals in (2.5*a–d*) are evaluated using the trapezoidal rule; in carrying out this procedure, the expression (2.1) is inverted by Newton iteration to obtain $y=y(\psi;a,b)$. For intermediate values of the quantity $a^2+b^2+a'^2+b'^2$, small-amplitude expansions of the kernels, correct to eighth order in $a$ and $b$, are used.

The numerical method described by (B 1)–(B 3) is applied at the interior points of the domain. At the far-field boundaries of the computational domain, $\xi_{\pm\infty}$ and $Y_\infty$, we set the wave amplitudes and their spatial derivatives to zero. Spurious reflections are eliminated by monitoring the disturbance amplitudes close to the boundaries and adding more points when they exceed a small critical value. On the boundary $Y=0$ ($j=0$), we obtain upon differentiating (2.7) with respect to $T$

$$a_T = b_T \tan\epsilon f + \epsilon f_T \left[ b \sec^2 \epsilon f - \tfrac{1}{2} \sec \epsilon f (1+\epsilon f \tan \epsilon f) \right]. \tag{B 4}$$

Substituting the expression (B 4) for $a_T$ into the discretized version of (4.1*b*), the values of $b_T$ on the boundary points may be determined. Similarly, $b_{TT}$ is determined using an expression analogous to the second of (B 3). The amplitude $a(\xi, Y=0)$ is then computed at the new time step using the boundary condition (2.7).

At each time step, the computation is commenced on $j=1$, the first point away from the boundary $Y=0$. Using the linearized versions of (4.1*a*, *b*), the values of $a$ and $b$ at $i=1$ (the first interior point from the left-hand boundary) are first determined, and the entire $(\xi, Y)$-plane is covered by consecutive $\xi$-sweeps. The values on the lower boundary $j=0$ are then computed using the procedure described earlier. Although this procedure works well for small topography amplitudes, slowly growing grid-scale oscillations were found to develop at larger amplitudes. As in Prasad *et al.* (1996), these oscillations were suppressed by using the 5-point smoothing formula of Shapiro (1975):

$$f_j = \tfrac{1}{16}(-f_{j-2} + 4f_{j-1} + 10f_j + 4f_{j+1} - f_{j+2}).$$

It was only necessary to apply this formula infrequently; moreover, the results were not dependent on the precise frequency with which the smoothing was applied.

## REFERENCES


Akylas, T. R. 1987 Nonlinear forced wave phenomena. In *Nonlinear Wave Interactions in Fluids* (ed. R. W. Miksad, T. R. Akylas & T. Herbert), vol. 87, p. 157. ASME-AMD.

Baines, P. G. 1995 *Topographic Effects in Stratified Flows.* Cambridge University Press.

Clarke, S. R. & Grimshaw, R. H. J. 1999 The effect of weak shear on finite-amplitude internal solitary waves. *J. Fluid Mech.* **395**, 125.

Dubreil-Jacotin, M. L. 1937 Sur les théorèmes d'existence relatifs aux ondes permanents périodiques à deux dimensions dans les liquides hétérogènes. *J. Maths Pure Appl.* **16**, 43.

Grimshaw, R. H. J., Chan, K. H. & Chow, K. W. 2002 Transcritical flow of a stratified fluid: the forced extended Korteweg–de Vries model. *Phys. Fluids* **14**, 755.

Grimshaw, R. H. J. & Smyth, N. 1986 Resonant flow of a stratified fluid over topography. *J. Fluid Mech.* **169**, 429.

Grimshaw, R. & Yi, X. 1991 Resonant generation of finite-amplitude waves by the flow of a uniformly stratified fluid over topography. *J. Fluid Mech.* **229**, 603.

Helfrich, K. R. & Melville, W. K. 1986 On long nonlinear internal waves over slope–shelf topography. *J. Fluid Mech.* **167**, 285.

Kakutani, T. & Yamasaki, N. 1978 Solitary waves on a two-layer fluid. *J. Phys. Soc. Japan* **45**, 674.

Kantzios, Y. D. & Akylas, T. R. 1993 An asymptotic theory of nonlinear stratified flow of large depth over topography. *Proc. R. Soc. Lond.* A **440**, 639 (referred to herein as KA).

Long, R. R. 1953 Some aspects of the flow of a stratified fluid. I. A theoretical investigation. *Tellus* **5**, 42.

Miles, J. W. 1979 On internal solitary waves. *Tellus* **31**, 456.

Phillips, O. M. 1968 The interaction trapping of internal gravity waves. *J. Fluid Mech.* **34**, 407.

Prasad, D., Ramirez, J. & Akylas, T. R. 1996 Stability of stratified flow of large depth over finite-amplitude topography. *J. Fluid Mech.* **320**, 369.

Rottman, J. W., Broutman, D. & Grimshaw, R. 1996 Numerical simulations of uniformly stratified fluid flow over topography. *J. Fluid Mech.* **306**, 1.

Shapiro, R. 1975 Linear filtering. *Maths Comput*. **29**, 1094.